



HAL
open science

Stable Model Predictive Strategy for Rendezvous Hovering Phases Allowing for Control Saturation

Paulo Ricardo Arantes Gilz, Mioara Joldes, Christophe Louembet, Frédéric Camps

► **To cite this version:**

Paulo Ricardo Arantes Gilz, Mioara Joldes, Christophe Louembet, Frédéric Camps. Stable Model Predictive Strategy for Rendezvous Hovering Phases Allowing for Control Saturation. 2018. hal-01678768v1

HAL Id: hal-01678768

<https://hal.science/hal-01678768v1>

Preprint submitted on 9 Jan 2018 (v1), last revised 5 Nov 2018 (v2)

HAL is a multi-disciplinary open access archive for the deposit and dissemination of scientific research documents, whether they are published or not. The documents may come from teaching and research institutions in France or abroad, or from public or private research centers.

L'archive ouverte pluridisciplinaire **HAL**, est destinée au dépôt et à la diffusion de documents scientifiques de niveau recherche, publiés ou non, émanant des établissements d'enseignement et de recherche français ou étrangers, des laboratoires publics ou privés.

Stable Model Predictive Strategy for Rendezvous Hovering Phases Allowing for Control Saturation

Paulo R. Arantes Gilz*, Mioara Joldes†, Christophe Louembet‡, Frédéric Camps§

LAAS-CNRS, Université de Toulouse, CNRS, Toulouse, France

Abstract

This paper presents a model predictive control strategy for the hovering phases of the impulsive spacecraft rendezvous problem producing a convergent sequence of relative trajectories, even under propellers saturation constraints. Adopting a linearized dynamics for the relative spacecraft dynamics, we present a parametrization of the relative trajectories. This parametrization and the constraints describing the hovering zones are employed in the formulation of the impulsive fuel-optimal control strategy, which is then proved to be stable. Numerical methods are proposed to solve the optimization problems characterizing each call of the controller. Finally, hardware-in-the-loop simulations using a synthesized LEON3 microprocessor and linear and disturbed nonlinear models for the relative dynamics are performed to assess the efficiency and robustness of the proposed approach.

1 Introduction

Mastering the spacecraft rendezvous was crucial during the space conquest era and nowadays opens new economical opportunities for the space industry. In fact, numerous space tugs have been developed by the different actors in this industry. In particular, a key feature for mission success is the autonomy: the ability of the involved spacecraft to compute their guidance and control commands without human intervention.

The work presented in this paper aims to design a consumption-optimal controller compatible with the performance of a space flight certified computation board. We focus on the phases of the rendezvous problem in which a chaser spacecraft must keep station inside a restricted tolerance zone in space (we assume a rectangular cuboid) defined in the body-fixed frame of a leader spacecraft - these are the so-called “hovering” phases [16]. In this work, the hovering phases are controlled by means of chemical thrusters and the control actions are modeled as impulsive velocity corrections. In previous works, we addressed this problem from two different points of view. In [7], several linear control laws based on the dynamical hybrid systems theory have been developed. However, such approaches are not able to account for any constraints on the state or command despite their proven ability to stabilize the chaser vehicle around a given relative orbit. In [2, 3], the hovering control is achieved by means of predictive control laws accounting for input saturation conditions and polytopic constraints on the relative position. The proposed work improves and expands on these MPC-oriented papers.

Since the early years of 2000, the model predictive control (MPC) schemes for impulsive spacecraft rendezvous have been developed in the aim of providing fuel-thrifty and sustainable control algorithm. The model predictive control is here thought as closed loop control scheme that embeds the resolution of an optimal control on a receding horizon. This control scheme is named *implicit closed-loop* [23, 11]. In the context of space relative motion, the advantage of such control scheme is to minimize the consumption

*PhD Graduate, Methods et Algorithms in Control, 7 Avenue du Colonel Roche; currently Université de Toulouse, Université Paul Sabatier, Laboratoire d'Analyse et d'Architectures des Systèmes, F-31400 Toulouse, France; prarante@laas.fr

†Researcher, Methods et Algorithms in Control, 7 Avenue du Colonel Roche; currently Université de Toulouse, Université Paul Sabatier, Laboratoire d'Analyse et d'Architectures des Systèmes, F-31400 Toulouse, France; mjoldes@laas.fr

‡Associate Professor, Methods et Algorithms in Control, 7 Avenue du Colonel Roche; currently Université de Toulouse, Université Paul Sabatier, Laboratoire d'Analyse et d'Architectures des Systèmes, F-31400 Toulouse, France; louembet@laas.fr

§Research Engineer, Methods et Algorithms in Control, 7 Avenue du Colonel Roche; currently Université de Toulouse, Université Paul Sabatier, Laboratoire d'Analyse et d'Architectures des Systèmes, F-31400 Toulouse, France; fcamps@laas.fr

while accounting for restrictions and constraints arisen from technological and safety requirements in addition to provide robust stability to identified perturbations [6]. In the framework of a chemical propulsion and its impulsive modeling, the literature is rich of examples of model predictive controller that can be cast into several categories according to [23].

A first implicit closed-loop approach known as *open-loop min-max MPC* is based on the resolution of an inner uncertain optimal control problems as in [22, 25]. Such MPC approach has been successful in relative motion impulsive control in presence of navigation errors [13]. If robust stability can be derived [21], all good properties of such control schemes collapse if the feasible recursion (*i.e.*, the case in which all inner programs are feasible) can not be established. A second approach, called *constraint tightening MPC*, is designed to ensure the recursive feasibility by *a priori* tightening the constraints on the predicted states [17]. This approach has been developed mainly for linear time invariant systems and necessitates either the existence of stabilizing state-feedback controller [6, 28] or off-line computation [17, 30]. However, saturations are not explicitly considered in cited works. Moreover, such control schemes are difficult to apply to time varying dynamics derived from elliptical relative motion. In another approach, the so-called *feedback MPC*, the decision variables are the feedback policies instead of the control value. With such approach, the MPC control avoids the open-loop propagation of the uncertainties and limits the spread of perturbed trajectories[18]. Considering affine state feedback policies, the *tube-based MPC* is derived [20, 24] where the computations are usually made off-line. Such approach has been applied to rendezvous guidance and control problem in [9] while considering a fixed-time horizon.

In this work, we develop an implicit closed-loop MPC algorithm. Our strategy aims at maintaining the chaser in a given window thanks to periodic motion as proposed in the recent work [29]. However, we particularly control the relative motion around window-included free periodic orbits described in [10], contrarily to the forced orbits exploited in [29]. The periodic orbits of interest have been described in [10] in terms positive polynomial certification and in [3] as a semi-algebraic set.

Our contribution consists also in providing the readers an MPC controller for which stability is proved even when the presence of saturation constraints on controls may make the space window unreachable from the current state. A second contribution is the performance of extensive numerical results that aim to highlight the efficiency of the MPC controller in terms of control quality and numerical burden. Following the FPGA framework of the tests carried out in [14, 15], the simulations presented herein are executed in a hardware-in-the-loop fashion, where the control computation is executed on a synthesized FPGA LEON3 board certified for spacecraft usage.

2 Modeling the rendezvous hovering phases problem

In this section we present the assumptions and equations employed in the modeling of the linearized relative dynamics between spacecraft. Once this model is obtained, by performing transformations of the state variable, a parametrization of the periodic space-constrained relative trajectories is deduced. These developments are employed in Sections 3 for the formulation of the MPC scheme and its stability proof, as well as in Section 4.2 for the conception of semi-algebraic check functions for the space constraints.

2.1 Relative spacecraft motion

Figure 1 presents the frames used to model the relative motion between the leader S_l and the follower S_f spacecrafts. The Earth-Centered Inertial and the Local Vertical / Local Horizontal frames are respectively given by $\{O, \vec{I}, \vec{J}, \vec{K}\}$ and $\{S_l, \vec{x}, \vec{y}, \vec{z}\}$.

The angle ν , between the direction of perigee and the leader's position, is the true anomaly, $0 < e < 1$ is the leader orbit eccentricity, a is the leader orbit semi-major axis and μ is Earth's gravitational constant. Considering that $\|\vec{OS}_l\| \gg \|\vec{S}_l\vec{S}_f\|$ and assuming Keplerian orbits, the relative dynamics can be linearized

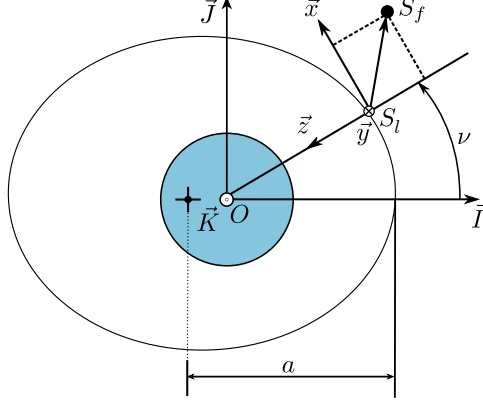


Figure 1: Inertial and relative frames

and described by the simplified linearized Tschauner-Hempel equations [32, 35]:

$$\tilde{X}'_{xz}(\nu) = \underbrace{\begin{bmatrix} 0 & 0 & 1 & 0 \\ 0 & 0 & 0 & 1 \\ 0 & 0 & 0 & 2 \\ 0 & \frac{3}{\rho_\nu} & -2 & 0 \end{bmatrix}}_{\tilde{A}_{xz}(\nu)} \tilde{X}_{xz}(\nu), \quad \tilde{X}'_y(\nu) = \underbrace{\begin{bmatrix} 0 & 1 \\ -1 & 0 \end{bmatrix}}_{\tilde{A}_y(\nu)} \tilde{X}_y(\nu), \quad (2.1)$$

where $\rho_\nu = \rho(\nu) = (1 + e \cos \nu)$. In (2.1) we explicitly split the equations to emphasize the fact that the so-called in-plane motion (xz -plane) is decoupled from the out-of-plane motion (y -axis). For a given time t , the change of variable from the LVLH state $X(t) = [x(t), y(t), z(t), \dot{x}(t), \dot{y}(t), \dot{z}(t)]^T$ to the $\tilde{X}(\nu)$ vector can be performed via the following transformation:

$$\tilde{X}(\nu) = T(\nu)X(t), \quad \text{with} \quad T(\nu) = \begin{bmatrix} \rho_\nu \mathbb{I}_3 & 0_3 \\ \rho'_\nu \mathbb{I}_3 & (k^2 \rho_\nu)^{-1} \mathbb{I}_3 \end{bmatrix}, \quad (2.2)$$

where $(\cdot)' = \frac{d(\cdot)}{d\nu}$ and $k^2 = \sqrt{\frac{\mu}{a^3(1-e^2)^3}}$.

During the rendezvous hovering phases, the follower spacecraft is required to remain in the interior of a certain limited region of the space. We assume in the sequel that this hovering range is a rectangular cuboid (tolerance box):

$$\underline{x} \leq x(t) \leq \bar{x} \quad \underline{y} \leq y(t) \leq \bar{y} \quad \underline{z} \leq z(t) \leq \bar{z}, \quad \forall t \geq t_0. \quad (2.3)$$

Another variable change is performed in order to obtain a better-suited representation of these constrained relative trajectories, with the advantage of providing a physical description of the relative orbits, contrary to the states X and \tilde{X} that only give the instantaneous position and velocity. The new state, the so-called *vector of parameters* for the spacecraft relative motion, is defined as (see [8, 10] for details):

$$D(\nu) = [d_0(\nu), d_1(\nu), d_2(\nu), d_3(\nu), d_4(\nu), d_5(\nu)]^T \quad (2.4)$$

and can also be split into two vectors representing respectively the in-plane and the out-of-plane motion: $D_{xz}(\nu) = [d_0(\nu), d_1(\nu), d_2(\nu), d_3(\nu)]^T$ and $D_y(\nu) = [d_4(\nu), d_5(\nu)]^T$.

These parameters can be expressed in function of \tilde{X} as follows:

$$D_{xz}(\nu) = \frac{1}{e^2 - 1} \underbrace{\begin{bmatrix} 0 & -(3ec_\nu + e^2 + 2) & \rho_\nu^2 & -es_\nu \rho_\nu \\ 0 & 3(e + c_\nu) & -(2c_\nu + ec_\nu^2 + e) & s_\nu \rho_\nu \\ 0 & \frac{3s_\nu(\rho_\nu + e^2)}{\rho_\nu} & -s_\nu(2 + ec_\nu) & 2e - c_\nu \rho_\nu \\ 1 & \frac{-3es_\nu(2 + ec_\nu)}{\rho_\nu} & es_\nu(2 + ec_\nu) & ec_\nu \rho_\nu - 2 \end{bmatrix}}_{C_{xz}(\nu)} \tilde{X}_{xz}(\nu), \quad D_y(\nu) = \underbrace{\begin{bmatrix} c_\nu & -s_\nu \\ s_\nu & c_\nu \end{bmatrix}}_{C_y(\nu)} \tilde{X}_y(\nu), \quad (2.5)$$

where $s_\nu = \sin(\nu)$ and $c_\nu = \cos(\nu)$.

By manipulating equations (2.1) and (2.5) (see [8] for details), one can obtain the following dynamical system representing the evolution of the vector of parameters:

$$D'_{xz}(\nu) = \underbrace{\begin{bmatrix} 0 & 0 & 0 & 0 \\ 0 & 0 & 0 & 0 \\ -\frac{3e}{\rho_\nu^2} & 0 & 0 & 0 \\ \frac{3}{\rho_\nu^2} & 0 & 0 & 0 \end{bmatrix}}_{A_{D_{xz}}(\nu)} D_{xz}(\nu), \quad D'_y(\nu) = \underbrace{\begin{bmatrix} 0 & 0 \\ 0 & 0 \end{bmatrix}}_{A_{D_y}(\nu)} D_y(\nu), \quad (2.6)$$

which can also be described by its transition matrix:

$$D_{xz}(\nu) = \underbrace{\begin{bmatrix} 1 & 0 & 0 & 0 \\ 0 & 1 & 0 & 0 \\ -3e\mathcal{J}_{\nu_0}(\nu) & 0 & 1 & 0 \\ 3\mathcal{J}_{\nu_0}(\nu) & 0 & 0 & 1 \end{bmatrix}}_{\Phi_{D_{xz}}(\nu, \nu_0)} D_{xz}(\nu_0), \quad D_y(\nu) = \underbrace{\begin{bmatrix} 1 & 0 \\ 0 & 1 \end{bmatrix}}_{\Phi_{D_y}(\nu, \nu_0)} D_y(\nu_0), \quad (2.7)$$

where $\mathcal{J}_{\nu_0}(\nu)$ is given by:

$$\mathcal{J}_{\nu_0}(\nu) := \int_{\nu_0}^{\nu} \frac{d\tau}{\rho(\tau)^2} = \sqrt{\frac{\mu}{a^3}} \frac{t - t_0}{(1 - e^2)^{3/2}}. \quad (2.8)$$

Remark 2.1. Hereafter we use the notation $C(\nu)$, $A_D(\nu)$ and $\Phi_D(\nu_N, \nu_i)$ to refer to the concatenation of the respective in-plane and out-of-plane matrices.

In what follows, the problem constraints are presented. They intervene in the constrained fuel-optimal control problem that is to be solved at each call of the model predictive controller.

2.2 Space constrained periodic relative trajectories

One is interested in obtaining periodic trajectories, since this guarantees that the relative motion remains bounded in absence of disturbances. However, the relative trajectories described by (2.1) are not periodic in general. By imposing $\tilde{X}(\nu + 2\pi) = \tilde{X}(\nu)$, $\forall \nu$ one can deduce that a necessary and sufficient condition for this constraint to be respected is:

$$d_0(\nu_0) = 0. \quad (2.9)$$

Remark 2.2. The condition $d_0(\nu_0) = 0$ is straightforwardly deduced, since the only non-periodic and divergent term $\mathcal{J}_{\nu_0}(\nu)$ in the relative motion equations always appears multiplied by d_0 :

$$\begin{aligned} \tilde{x}(\nu) &= (2 + e c_\nu)(d_1(\nu_0) s_\nu - d_2(\nu_0) c_\nu) + d_3(\nu_0) + 3(1 + e c_\nu)^2 \mathbf{d}_0(\nu_0) \mathcal{J}_{\nu_0}(\nu), \\ \tilde{z}(\nu) &= (1 + e c_\nu)(d_2(\nu_0) s_\nu + d_1(\nu_0) c_\nu - 3e s_\nu \mathbf{d}_0(\nu_0) \mathcal{J}_{\nu_0}(\nu)) + 2d_0(\nu_0). \end{aligned}$$

Remark 2.3. A notable property of periodic trajectories is that the vector of parameters $D(\nu)$ remains constant for any value of ν since its dynamic matrix $A_D(\nu)$ has non-zero values only in its first column (see (2.6)).

By imposing $d_0 = 0$ (periodicity condition) and using (2.2) and (2.5), the inequalities in (2.3) are rewritten as:

$$\begin{aligned} \underline{x} &\leq F_x(\nu)^T D_{xz} \leq \bar{x} & F_x(\nu) &= \begin{bmatrix} 0, & \frac{(2+e c_\nu)s_\nu}{1+e c_\nu}, & \frac{-(2+e c_\nu)c_\nu}{1+e c_\nu}, & \frac{1}{1+e c_\nu} \end{bmatrix}^T \\ \underline{y} &\leq F_y(\nu)^T D_y \leq \bar{y}, \quad \forall \nu, & F_z(\nu) &= \begin{bmatrix} 0, & c_\nu, & s_\nu, & 0 \end{bmatrix}^T \\ \underline{z} &\leq F_z(\nu)^T D_{xz} \leq \bar{z} & F_y(\nu) &= \begin{bmatrix} \frac{c_\nu}{1+e c_\nu}, & \frac{s_\nu}{1+e c_\nu} \end{bmatrix}^T \end{aligned} \quad (2.10)$$

The admissible set i.e., the set of periodic trajectories satisfying the inequalities in (2.10), is then defined as:

$$S_D := \left\{ D \in \mathbb{R}^6 \mid d_0 = 0, \begin{array}{l} \underline{x} \leq F_x(\nu)^T D_{xz} \leq \bar{x} \\ \underline{y} \leq F_y(\nu)^T D_y \leq \bar{y} \\ \underline{z} \leq F_z(\nu)^T D_{xz} \leq \bar{z} \end{array}, \forall \nu \right\}, \quad (2.11)$$

and since the out-of-plane and in-plane dynamics can be decoupled, we also define:

$$S_{D_y} = \{D_y \in \mathbb{R}^2 \mid \underline{y} \leq F_y(\nu)^T D_y \leq \bar{y}, \forall \nu\}, \quad (2.12)$$

$$S_{D_{xz}} = \left\{ D_{xz} \in \mathbb{R}^4 \mid d_0 = 0, \begin{array}{l} \underline{x} \leq F_x(\nu)^T D_{xz} \leq \bar{x} \\ \underline{z} \leq F_z(\nu)^T D_{xz} \leq \bar{z} \end{array}, \forall \nu \right\}. \quad (2.13)$$

Proposition 2.1. *The admissible set S_D is convex and bounded.*

Proof. The convexity can be straightforwardly proven by showing that any convex combination of two elements of S_D also belongs to S_D . In order to prove the boundedness of the set, we evaluate the inequalities in (2.11) at specific values:

Computing the bounds for d_1 and d_2 : by evaluating the z inequalities at $\nu = 0$ and $\nu = \frac{\pi}{2}$, we obtain:

$$\underline{z} \leq d_1 \leq \bar{z} \quad (2.14)$$

$$\underline{z} \leq d_2 \leq \bar{z} \quad (2.15)$$

Computing the bounds for d_3 : by evaluating the x inequalities at $\nu = 0$, $\nu = \frac{2\pi}{3}$ and $\nu = \frac{4\pi}{3}$ and manipulating the produced inequalities, we obtain:

$$\underline{x} \left(\frac{4+e-e^2}{4+e} \right) \leq d_3 \leq \bar{x} \left(\frac{4+e-e^2}{4+e} \right) \quad (2.16)$$

Computing the bounds for d_4 and d_5 : by evaluating the y inequalities at $\nu = 0$ and $\nu = \frac{\pi}{2}$, we obtain:

$$\underline{y}(1+e) \leq d_4 \leq \bar{y}(1+e) \quad (2.17)$$

$$\underline{y} \leq d_5 \leq \bar{y} \quad (2.18)$$

Then, since any element of S_D is entry-wise bounded, the set S_D is itself bounded. ■

The description of the admissible set previously presented consists in the evaluation of infinitely many affine inequalities on the vector of parameters, which depends on ν . Although theoretically interesting, this description is not practical from a numerical point of view, since the infinitely many constraints are hard to be accounted for, when employed in the formulation of optimization problems. In Section 4, alternative finite descriptions are presented and employed.

2.3 Propellers, fuel-consumption and saturation

We suppose that the follower spacecraft has six identical thrusters, one pair symmetrically and oppositely disposed by axis, as indicated in Fig. 2:

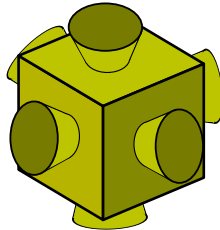


Figure 2: Propellers arrangement

We consider the employment of chemical propellers producing instantaneous impulsive velocity corrections ΔV . Given that, the fuel consumption is then modeled as the sum of the absolute value of the thrusts applied in each direction:

$$J(\Delta V) = \sum_{i=1}^N \|\Delta V(\nu_i)\|_1 = \sum_{i=1}^N |\Delta V_x(\nu_i)| + |\Delta V_y(\nu_i)| + |\Delta V_z(\nu_i)|, \quad (2.19)$$

and assuming that the saturation threshold for each propeller is $\overline{\Delta V} > 0$, this constraint is written as:

$$|\Delta V_x(\nu_i)| \leq \overline{\Delta V}, \quad |\Delta V_y(\nu_i)| \leq \overline{\Delta V}, \quad |\Delta V_z(\nu_i)| \leq \overline{\Delta V}. \quad (2.20)$$

For a given true anomaly value ν , the state right after an impulse $\Delta V(\nu) = [\Delta V_x(\nu), \Delta V_y(\nu), \Delta V_z(\nu)]^T$ is defined as $X^+(\nu)$ and can be computed by:

$$X^+(\nu) = X(\nu) + B \Delta V(\nu), \quad B = [0_3 \ \mathbb{I}_3]^T. \quad (2.21)$$

Performing the variable changes $X(\nu) \xrightarrow{(2.2)} \tilde{X}(\nu) \xrightarrow{(2.5)} D(\nu)$, the parameter vector after the impulse $D^+(\nu)$ is given by:

$$D^+(\nu) = D(\nu) + C(\nu)T(\nu)B \Delta V(\nu). \quad (2.22)$$

Using the transition matrices given in (2.7), the vector of parameters right after a sequence of impulses applied at $\nu_1 \dots \nu_{N-1}, \nu_N$ can be expressed as follows:

$$D^+(\nu_N) = \Phi_D(\nu_N, \nu_1)D(\nu_1) + \sum_{i=1}^N \underbrace{\Phi_D(\nu_N, \nu_i)C(\nu_i)T(\nu_i)B}_{B_D(\nu_N, \nu_i)} \Delta V(\nu_i) \quad (2.23)$$

or, similarly, by splitting the dynamics into out-of-plane and in-plane motion, we obtain:

$$\begin{aligned} D_{xz}^+(\nu_N) &= \Phi_{D_{xz}}(\nu_N, \nu_1)D_{xz}(\nu_1) + \sum_{i=1}^N B_{D_{xz}}(\nu_N, \nu_i) \Delta V_{xz}(\nu_i), \\ D_y^+(\nu_N) &= \Phi_{D_y}(\nu_N, \nu_1)D_y(\nu_1) + \sum_{i=1}^N B_{D_y}(\nu_N, \nu_i) \Delta V_y(\nu_i), \end{aligned} \quad (2.24)$$

where $\Delta V_{xz}(\nu_i) = [\Delta V_x(\nu_i), \Delta V_z(\nu_i)]^T$,

$$\begin{aligned} B_{D_{xz}}(\nu_N, \nu) &= \frac{1}{k^2(e^2 - 1)\rho_\nu} \begin{bmatrix} \rho_\nu^2 & -es_\nu\rho_\nu \\ -(2c_\nu + ec_\nu^2 + e) & s_\nu\rho_\nu \\ -s_\nu(2 + ec_\nu) - 3e\mathcal{J}_\nu(\nu_N) & 2e - c_\nu\rho_\nu + 3e^2s_\nu\rho_\nu\mathcal{J}_\nu(\nu_N) \\ es_\nu(2 + ec_\nu) + 3\mathcal{J}_\nu(\nu_N) & ec_\nu\rho_\nu - 2 - 3es_\nu\rho_\nu\mathcal{J}_\nu(\nu_N) \end{bmatrix}, \\ B_{D_y}(\nu_N, \nu) &= \frac{1}{k^2\rho_\nu} \begin{bmatrix} -s_\nu \\ c_\nu \end{bmatrix}. \end{aligned} \quad (2.25)$$

By introducing the matrices:

$$\begin{aligned} M(\nu_1, \dots, \nu_N) &:= [B_D(\nu_N, \nu_1), \dots, B_D(\nu_N, \nu_N)], \\ M_{xz}(\nu_1, \dots, \nu_N) &:= [B_{D_{xz}}(\nu_N, \nu_1), \dots, B_{D_{xz}}(\nu_N, \nu_N)], \\ M_y(\nu_1, \dots, \nu_N) &:= [B_{D_y}(\nu_N, \nu_1), \dots, B_{D_y}(\nu_N, \nu_N)], \end{aligned}$$

and the vectors:

$$\begin{aligned} \Delta V &:= [\Delta V(\nu_1), \dots, \Delta V(\nu_N)]^T, \\ \Delta V_{xz} &:= [\Delta V_x(\nu_1), \Delta V_z(\nu_1) \dots \Delta V_x(\nu_N), \Delta V_z(\nu_N)]^T, \\ \Delta V_y &:= [\Delta V_y(\nu_1), \dots, \Delta V_y(\nu_N)]^T, \end{aligned}$$

expressions (2.23) and (2.24) can be further simplified:

$$\begin{aligned} D^+(\nu_N) &= \Phi_D(\nu_N, \nu_1)D(\nu_1) + M(\nu_1, \dots, \nu_N) \Delta V, \\ D_{xz}^+(\nu_N) &= \Phi_{D_{xz}}(\nu_N, \nu_1)D_{xz}(\nu_1) + M_{xz}(\nu_1, \dots, \nu_N) \Delta V_{xz}, \\ D_y^+(\nu_N) &= \Phi_{D_y}(\nu_N, \nu_1)D_y(\nu_1) + M_y(\nu_1, \dots, \nu_N) \Delta V_y. \end{aligned} \quad (2.26)$$

2.4 Fuel-optimal impulsive control problem

Once the mathematical models for the evolution of the vector of parameters and for the constraints are obtained (Sections 2.2 and 2.3), we can formulate the fuel-optimal impulsive control problem that is solved at each call of the MPC algorithm:

Problem 1. Given $N \geq 3$, $\nu_1 < \dots < \nu_N \in \mathbb{R}_{>0}$, $D(\nu_1) \in \mathbb{R}^6$, $e, a, \mu \in \mathbb{R}$, find $\Delta V^* \in \mathbb{R}^{3N}$ such that:

$$\begin{aligned} \Delta V^* = \operatorname{argmin}_{\Delta V} \quad & J(\Delta V) \\ \text{s.t.} \quad & \begin{cases} D(\nu_1) = D_1 \\ D^+(\nu_N) = \Phi_D(\nu_N, \nu_1)D(\nu_1) + M(\nu_1, \dots, \nu_N) \Delta V \\ d_0^+(\nu_N) = 0 \\ D^+(\nu_N) \in S_D \end{cases} \end{aligned} \quad (\mathcal{P})$$

In the sequel we show that the periodicity equality constraint $d_0^+(\nu_N) = 0$ can be dropped by considering only the impulsive velocity corrections that produce periodic relative trajectories. The idea is to construct a basis for the affine subspace to which the vectors of impulsive velocity corrections such that $d_0^+(\nu_N) = 0$ belong. In order to do so, let us begin by rewriting the first line of (2.23):

$$d_0^+(\nu_N) = d_0(\nu_1) + \sum_{i=1}^N \frac{1}{k^2(e^2 - 1)} [\rho_{\nu_i} \quad -e s_{\nu_i}] \Delta V_{xz}(\nu_i). \quad (2.27)$$

By defining the row vector

$$M_0(\nu_1, \dots, \nu_N) := \frac{1}{k^2(e^2 - 1)} [\rho_{\nu_1}, \quad -e s_{\nu_1}, \quad \dots, \quad \rho_{\nu_N}, \quad -e s_{\nu_N}],$$

we can rewrite the equation (2.27) as:

$$d_0^+(\nu_N) = d_0(\nu_1) + M_0(\nu_1, \dots, \nu_N) \Delta V_{xz}. \quad (2.28)$$

Then we express ΔV_{xz} as:

$$\Delta V_{xz}(\lambda) = \underbrace{\begin{bmatrix} | & & | \\ v_1 & \dots & v_{2N-1} \\ | & & | \end{bmatrix}}_{M_0^\perp(\nu_1, \dots, \nu_N)} \lambda + \Delta V_0, \quad (2.29)$$

where $\Delta V_0 \in \mathbb{R}^{2N}$ is an arbitrary sequence of in-plane impulses producing a periodic relative trajectory and $M_0^\perp(\nu_1, \dots, \nu_N)\lambda$ represents a linear combination of the v_i vectors belonging to the kernel of the row vector $M_0(\nu_1, \dots, \nu_N)$, given by:

$$v_i := \left[\underbrace{0, \dots, 0}_{(i-1) \text{ zeros}}, \quad a_{i+1}, \quad -a_i, \quad \underbrace{0, \dots, 0}_{(2N-1-i) \text{ zeros}} \right]^T, \quad (2.30)$$

where a_i is the i -th entry of $M_0(\nu_1, \dots, \nu_N)$.

Problem (\mathcal{P}) accounts for both the in-plane and out-of-plane dynamics, even though they can be solved separately (in Section 3, these dynamics are split and represented by the functions γ_{xz} and γ_y respectively). Moreover, one can remark that the control actions are not saturated in the formulation of (\mathcal{P}); an *ad hoc* function $\gamma_{\Delta V}$ is employed to take these constraints into account in the following.

3 Model Predictive Control Strategy

In this section we present the model predictive control strategy that computes sequences of impulses generating a sequence of states $(D_k)_{k \in \mathbb{N}}$ that, even under saturation of the actuators, iteratively converges to a state belonging to a given non-empty admissible set S_D .

The main ideas used in the conception of this strategy, which is formally summarized in Algorithm 1, are the following ones:

Periodic trajectories produce no drift. Let us recall the transition matrix for the in-plane motion:

$$D_{xz}(\nu) = \underbrace{\begin{bmatrix} 1 & 0 & 0 & 0 \\ 0 & 1 & 0 & 0 \\ -3e\mathcal{J}_{\nu_0}(\nu) & 0 & 1 & 0 \\ 3\mathcal{J}_{\nu_0}(\nu) & 0 & 0 & 1 \end{bmatrix}}_{\Phi_{D_{xz}}(\nu, \nu_0)} D_{xz}(\nu_0). \quad (3.1)$$

Remark that if $d_0(\nu_0) = 0$ the vector of parameters does not evolve within time. In order to eliminate this “drift” effect and keep the distance between the vector of parameters and the admissible set constant, Algorithm 1 first focuses on bringing d_0 to 0 (see Fig. 3).

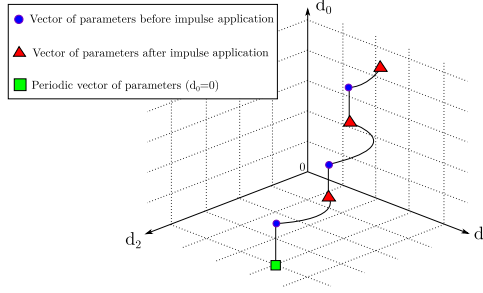


Figure 3: Generation of a periodic trajectory: between the triangle and the circle, the vector of parameters evolves in a plane $d_0 = \text{constant}$ parallel to the plane $d_2 \times d_3$; an impulsive velocity correction applied with the goal of reducing the absolute value of d_0 is represented by the vertical line linking a circle and a triangle; the square represents a vector of parameters describing a periodic trajectory (it does not evolve within time).

To achieve periodicity, one impulse would always be sufficient if the saturation conditions were met:

Proposition 3.1 (Minimal periodic impulse). *Let*

$$\begin{aligned} \gamma_p : \quad \mathbb{R} \times \mathbb{R} &\rightarrow \mathbb{R}^2 \\ d_{0_{xz}}(\nu_1), \nu_1 &\mapsto \underset{s.t.}{\operatorname{argmin}}_{\Delta V_{xz}} \|\Delta V_{xz}\|_1 \\ &\quad d_{0_{xz}}^+(\nu_1) = d_{0_{xz}}(\nu_1) + M_0(\nu_1)\Delta V_{xz}(\nu_1) = 0 \end{aligned} \quad (3.2)$$

Then, for any set of inputs, the function γ_p is well-defined in the sense that the feasible set of the minimization problem is not empty.

Proof. The line vector $M_0(\nu_1)$ has the following expression:

$$M_0(\nu_1) = (k^2(e^2 - 1))^{-1} \begin{bmatrix} 1 + e \cos(\nu_1) & -e \sin(\nu_1) \end{bmatrix}$$

and since the term $1 + e \cos(\nu_1) \neq 0$, $\forall \nu_1$ (because $0 < e < 1$), it is always possible to set:

$$\Delta V_{xz} = k^2(e^2 - 1) \begin{bmatrix} -\frac{d_{0_{xz}}(\nu_1)}{1 + e \cos(\nu_1)} & 0 \end{bmatrix}^T,$$

satisfying the equation $0 = d_{0_{xz}}(\nu_1) + M_0(\nu_1)\Delta V_{xz}$. ■

Remark 3.1. *Since the minimization problem in (3.2) contains ℓ_1 -norm criteria (which are not strictly convex), infinitely many solutions may exist. In order to enforce unicity, we could have taken the solution with minimal ℓ_2 -norm (which is strictly convex), but for the sake of brevity, we consider in the sequel that in these special cases only one minimum is arbitrarily chosen.*

To account for saturation, we define the following saturation function:

$$\begin{aligned} \gamma_{\overline{\Delta V}} : \quad \mathbb{R}^n \setminus \{\vec{0}\} &\rightarrow \mathbb{R}^n \\ v &\mapsto \frac{\overline{\Delta V}}{\|v\|_\infty} \cdot v, \end{aligned} \quad (3.3)$$

which is used to scale-down the impulses solutions of the optimization Problem (\mathcal{P}), when solved from Algorithm 1. These decoupled problems (lines 2 and 3) have at least one solution, as stated in the following propositions.

Proposition 3.2 (Minimal out-of-plane impulses). *Given $N \geq 3$, $\tau_I \in \mathbb{R}_{>0}$ s.t. $\forall k \in \mathbb{Z}_{>0}, \tau_I \neq k\pi$, and ν_1, \dots, ν_N s.t. $\nu_{k+1} = \nu_k + \tau_I$, let*

$$\begin{aligned} \gamma_y : \quad \mathbb{R}^2 \times \mathbb{R} \times \dots \times \mathbb{R} &\rightarrow \mathbb{R}^N \\ D_y(\nu_N), \nu_1, \dots, \nu_N &\mapsto \underset{s.t.}{\operatorname{argmin}}_{\Delta V_y} \|\Delta V_y\|_1 \\ &\quad D_y^+(\nu_N) = D_y(\nu_1) + M_y(\nu_1, \dots, \nu_N) \Delta V_y \in S_{D_y} \end{aligned} \quad (3.4)$$

Then, the function γ_y is well-defined in the sense that the feasible set of (3.4) is not empty, that is, $\forall D_y \in \mathbb{R}^2, D_y^ \in S_{D_y} \neq \emptyset, \exists \Delta V_y \in \mathbb{R}^N$ s.t. $D_y^* = D_y + M_y(\nu_1, \dots, \nu_N) \Delta V_y$.*

Proof. The matrix $M_y(\nu_1, \dots, \nu_N)$ has the following expression:

$$M_y(\nu_1, \dots, \nu_N) = k^{-2} \begin{bmatrix} -\frac{\sin(\nu_1)}{\rho(\nu_1)} & \cdots & -\frac{\sin(\nu_N)}{\rho(\nu_N)} \\ \frac{\cos(\nu_1)}{\rho(\nu_1)} & \cdots & \frac{\cos(\nu_N)}{\rho(\nu_N)} \end{bmatrix}.$$

This matrix has rank 2, since $\det(M_y(\nu_1, \nu_2)) = \frac{\sin(\nu_2 - \nu_1)}{\rho(\nu_1)\rho(\nu_2)} \neq 0$ because of the hypothesis on ν_1, \dots, ν_N . Then, $\forall D_y, D_y^* \in \mathbb{R}^2$ the vector $\Delta V_y = (M_y^T M_y)^{-1} M_y^T (D_y^* - D_y)$ is well-defined and satisfies $D_y^* = D_y + M_y(\nu_1, \dots, \nu_N) \Delta V_y$. This is also particularly true if $D_y^* \in S_{D_y} \neq \emptyset$. ■

Proposition 3.3 (Minimal in-plane impulses). *Given $N \geq 3$, $\tau_I \in \mathbb{R}_{>0}$ s.t. $\forall k \in \mathbb{Z}_{>0}, \tau_I \neq k\pi$ and ν_1, \dots, ν_N s.t. $\nu_{k+1} = \nu_k + \tau_I$, let*

$$\begin{aligned} \gamma_{xz} : \quad \mathbb{R}^4 \times \mathbb{R} \times \dots \times \mathbb{R} &\rightarrow \mathbb{R}^{2N} \\ D_{xz}(\nu_1), \nu_1, \dots, \nu_N &\mapsto \underset{s.t.}{\operatorname{argmin}}_{\Delta V_{xz}} \|\Delta V_{xz}\|_1 \\ &\quad D_{xz}^+(\nu_N) = D_{xz}(\nu_1) + M_{xz}(\nu_1, \dots, \nu_N) \Delta V_{xz} \in S_{D_{xz}} \end{aligned} \quad (3.5)$$

Then the function γ_{xz} is well-defined in the sense that the feasible set of (3.5) is not empty, that is, $\forall D_{xz} \in \mathbb{R}^4, D_{xz}^ \in S_{D_{xz}} \neq \emptyset, \exists \Delta V_{xz} \in \mathbb{R}^{2N}$ s.t. $D_{xz}^* = D_{xz} + M_{xz}(\nu_1, \dots, \nu_N) \Delta V_{xz}$.*

Proof. Let us choose ΔV_{xz} as in (2.29). As demonstrated in Proposition 3.1 it is always possible to set $d_{0_{xz}}^+$ to any arbitrary value with a single impulse. Since $M_0^\perp(\nu_1, \dots, \nu_N)\lambda$ has no influence on the first entry of $D_{xz}^* - D_{xz}$, we conclude that ΔV_0 can be chosen to set the first entry of $D_{xz}^* - D_{xz}$ to any arbitrary value.

Now, let us demonstrate that it is always possible to choose λ that allow us to set the other three entries of $D_{xz}^* - D_{xz}$ to any arbitrary values. Computing $M_{xz} M_0^\perp(\nu_1, \dots, \nu_N)$, we obtain:

$$M_{xz} M_0^\perp(\nu_1, \dots, \nu_N) = (k^6 (e^2 - 1)^2)^{-1} \begin{bmatrix} 0 & 0 & 0 & 0 & 0 & \dots & 0 & 0 \\ \frac{\sin(\nu_1)}{\rho(\nu_1)} & \star & \frac{\sin(\nu_2)}{\rho(\nu_2)} & \star & \frac{\sin(\nu_3)}{\rho(\nu_3)} & \dots & \star & \frac{\sin(\nu_N)}{\rho(\nu_N)} \\ -\frac{\cos(\nu_1)}{\rho(\nu_1)} & \star & -\frac{\cos(\nu_2)}{\rho(\nu_2)} & \star & -\frac{\cos(\nu_3)}{\rho(\nu_3)} & \dots & \star & -\frac{\cos(\nu_N)}{\rho(\nu_N)} \\ \frac{\rho(\nu_1)}{1+\rho(\nu_1)} & \star & \frac{\rho(\nu_2)}{1+\rho(\nu_2)} & \star & \frac{\rho(\nu_3)}{1+\rho(\nu_3)} & \dots & \star & \frac{\rho(\nu_N)}{1+\rho(\nu_N)} \\ \frac{1+\rho(\nu_1)}{\rho(\nu_1)} & \star & \frac{1+\rho(\nu_2)}{\rho(\nu_2)} & \star & \frac{1+\rho(\nu_3)}{\rho(\nu_3)} & \dots & \star & \frac{1+\rho(\nu_N)}{\rho(\nu_N)} \end{bmatrix}.$$

and this matrix has rank 3, since:

$$\det \left(\begin{bmatrix} \frac{\sin(\nu_1)}{\rho(\nu_1)} & \frac{\sin(\nu_2)}{\rho(\nu_2)} & \frac{\sin(\nu_3)}{\rho(\nu_3)} \\ -\frac{\cos(\nu_1)}{\rho(\nu_1)} & -\frac{\cos(\nu_2)}{\rho(\nu_2)} & -\frac{\cos(\nu_3)}{\rho(\nu_3)} \\ \frac{1+\rho(\nu_1)}{\rho(\nu_1)} & \frac{1+\rho(\nu_2)}{\rho(\nu_2)} & \frac{1+\rho(\nu_3)}{\rho(\nu_3)} \end{bmatrix} \right) = -2 \frac{\sin(\nu_2 - \nu_1) + \sin(\nu_3 - \nu_2) - \sin(\nu_3 - \nu_1)}{k^{18} (e^2 - 1)^6 \rho(\nu_1) \rho(\nu_2) \rho(\nu_3)} \quad (3.6)$$

$$= -8 \frac{\sin \frac{\nu_2 - \nu_1}{2} \sin \frac{\nu_3 - \nu_2}{2} \sin \frac{\nu_3 - \nu_1}{2}}{k^{18} (e^2 - 1)^6 \rho(\nu_1) \rho(\nu_2) \rho(\nu_3)} \neq 0, \quad (3.7)$$

because of the hypothesis on ν_1, \dots, ν_N .

This implies that $\forall D_{xz}, D_{xz}^* \in \mathbb{R}^4$ it is possible to chose λ and ΔV_0 in such a manner that $\Delta V_{xz}(\lambda) = M_0^\perp(\nu_1, \dots, \nu_N)\lambda + \Delta V_0$ satisfies $D_{xz}^* = D_{xz} + M_{xz}(\nu_1, \dots, \nu_N) \Delta V_{xz}$. This is also particularly true if $D_{xz}^* \in S_{D_{xz}} \neq \emptyset$. ■

Remark 3.2. *Similarly, in the minimization problems (3.4) and (3.5), one arbitrary minimum is chosen when the problem is not strictly convex.*

Saturated impulses can be used to bring the vector of parameters closer to the admissible set once periodicity is achieved : let be an arbitrary periodic relative trajectory parametrized by $D(\nu_1)$ and a sequence of impulses ΔV^* producing a trajectory $D^*(\nu_N)$ belonging to the admissible set S_D :

$$S_D \ni D^*(\nu_N) = \Phi_D(\nu_N, \nu_1)D(\nu_1) + M(\nu_1, \dots, \nu_N)\Delta V^*.$$

As previously discussed, since $D(\nu_1)$ is a periodic trajectory, $\Phi_D(\nu_N, \nu_1)D(\nu_1) = D(\nu_1)$ and we can rewrite the previous equation as:

$$D^*(\nu_N) = D(\nu_1) + M(\nu_1, \dots, \nu_N)\Delta V^*.$$

If this sequence of impulses is scaled by a real number η between 0 and 1 (representing the saturation), it generates a vector of parameters $D^\circ(\nu_N)$, given by:

$$D^\circ(\nu_N) = D(\nu_1) + \eta M(\nu_1, \dots, \nu_N)\Delta V^*.$$

This new vector of parameters $D^\circ(\nu_N)$ is closer to the admissible trajectory $D^*(\nu_N)$ than the original $D(\nu_1)$:

$$\|D^*(\nu_N) - D^\circ(\nu_N)\|_2 \leq \|D^*(\nu_N) - D(\nu_1)\|_2,$$

since $D^*(\nu_N) - D(\nu_1) = M(\nu_1, \dots, \nu_N)\Delta V^*$ and $D^*(\nu_N) - D^\circ(\nu_N) = (1 - \eta)M(\nu_1, \dots, \nu_N)\Delta V^*$;

It is possible to get closer and closer to the admissible set by iteratively applying at least three saturated impulses within a true anomaly interval different from multiples of π : this property is based on the fact that under these particular assumptions, the input matrices M_{xz} and M_y have full rank (details in Prop. 3.2 and 3.3).

Now that all the necessary functions are defined, Algorithm 1 describing the proposed model predictive control strategy is presented hereafter:

Algorithm 1: Model predictive control strategy

Require: $X(\nu_1), \overline{\Delta V}, S_D, \tau_S, \tau_P, \tau_I \in \mathbb{R}_{>0}$ s.t. $\forall k \in \mathbb{Z}_{>0}, \tau_I \neq k\pi, N \geq 3, \nu_1, \dots, \nu_N$ s.t. $\nu_{k+1} = \nu_k + \tau_I$

- 1 $D(\nu_1) \leftarrow C(\nu_1)T(\nu_1)X(\nu_1)$;
- 2 $\Delta V_{xz}^* \leftarrow \gamma_{xz}(D_{xz}(\nu_1), \nu_1, \dots, \nu_N)$;
- 3 $\Delta V_y^* \leftarrow \gamma_y(D_y(\nu_1), \nu_1, \dots, \nu_N)$;
- // If the saturation is violated by the in-plane impulses
- 4 **if** $\|\Delta V_{xz}^*\|_\infty > \overline{\Delta V}$ **then**
- // If the trajectory is periodic
- 5 **if** $d_{0_{xz}}(\nu_1) == 0$ **then**
- 6 | $\Delta V_{xz}^* \leftarrow \gamma_{\overline{\Delta V}}(\Delta V_{xz}^*)$
- // If the trajectory is not periodic
- 7 **else**
- 8 | $\Delta V_y^* \leftarrow 0$;
- 9 | $\Delta V_{xz}^* \leftarrow \gamma_p(d_{0_{xz}}(\nu_1), \nu_1)$;
- 10 | **if** $\|\Delta V_{xz}^*\|_\infty > \overline{\Delta V}$ **then**
- 11 | | $\Delta V_{xz}^* \leftarrow \gamma_{\overline{\Delta V}}(\Delta V_{xz}^*)$;
- 12 | **apply impulse** ΔV_{xz}^* and ΔV_y^* at ν_1
- 13 | $\nu_1 \leftarrow \nu_1 + \tau_P$; // wait τ_P before call algorithm again
- 14 | **stop** ; // end of algorithm
- 15 **end**
- // If the saturation is violated by the out-of-plane impulses
- 16 **if** $\|\Delta V_y^*\|_\infty > \overline{\Delta V}$ **then**
- 17 | $\Delta V_y^* \leftarrow \gamma_{\overline{\Delta V}}(\Delta V_y^*)$;
- 18 **end**
- 19 **apply impulses** ΔV_{xz}^* and ΔV_y^* at $\nu_1 \dots \nu_N$
- 20 $\nu_1 \leftarrow \nu_N + \tau_S$; // wait τ_S before call algorithm again
- 21 **stop** ; // end of algorithm

Algorithm 1 takes as input a relative state in the LVLH framework $X(\nu_1)$, a saturation threshold $\overline{\Delta V}$, a non-empty admissible set S_D described by $\underline{x}, \bar{x}, \underline{y}, \bar{y}, \underline{z}, \bar{z}$, a sequence of N true anomaly instants ν_1, \dots, ν_N equally spaced by τ_I , the true anomaly interval between impulses to generate a periodic trajectory τ_P and the true anomaly interval between sequences of impulses τ_S . Consecutive calls of this algorithm produce a pattern of impulsive velocity corrections similar to the one presented in Fig. 4.

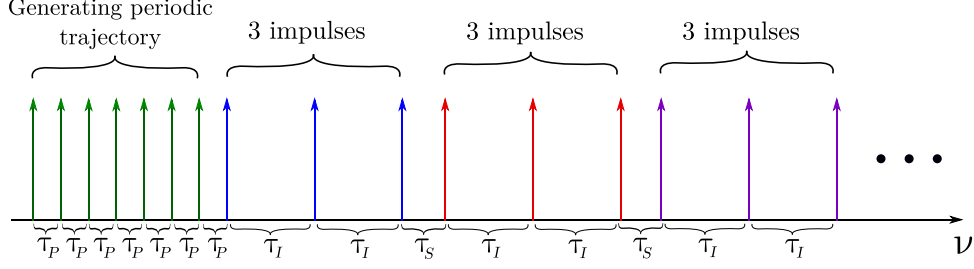


Figure 4: Pattern of impulsive velocity corrections along the true anomaly for a number of impulses $N = 3$.

3.1 Proof of convergence and invariance

In this section we prove the stability of previously described control strategy by demonstrating that the iterative application of the command actions computed in Algorithm 1 produces a sequence of states $(D_k)_{k \in \mathbb{N}}$ that converges to an element of S_D . Moreover, the admissible set is proved to be invariant under the action of the proposed controller, which guarantees that the state remains in the admissible set once the convergence is established.

In Algorithm 1, if no saturation occurs, the convergence of the state D to the admissible set S_D is trivial (by definition, one single call of γ_{xz} and γ_y is necessary to produce an admissible state D). However, for the cases in which the magnitude of the computed impulses goes beyond the saturation threshold, the stability proof is based on a geometrical property of convex sets: the idea is to prove that for a given convex $K \subset \mathbb{R}^n$ and any three elements $A, A', C \in \mathbb{R}^n$ such that $A \in \mathbb{R}^n \setminus K$, $C \in K$ and $A' = C + \lambda(A - C)$, $0 < \lambda < 1$, the distance from A to K is less than the distance from A' to K (in the sense of the norm $\|\cdot\|_2$):

Proposition 3.4. *Let be $K \subset \mathbb{R}^n$ convex, $A \in \mathbb{R}^n \setminus K$, $C \in K$, $B = \operatorname{argmin}_{\xi \in K} \|\xi - A\|_2$, $0 < \lambda < 1$, $A' = C + \lambda(A - C)$, $B' = \operatorname{argmin}_{\xi \in K} \|\xi - A'\|_2$. Then, $\operatorname{dist}(A') = \|B' - A'\|_2 < \|B - A\|_2 = \operatorname{dist}(A)$.*

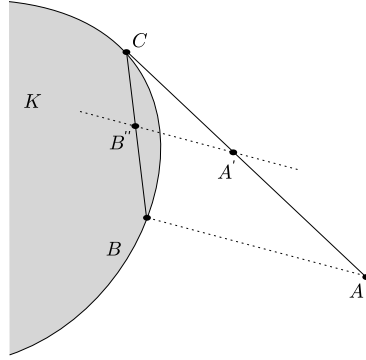


Figure 5: Illustration of points A, A', B, B'', C and convex K

Proof. We define $B'' = C + \lambda(B - C)$ (see Figure 5). Since K is convex and B'' is between B and C , $B'' \in K$. By developing the difference $B'' - A'$, we have that:

$$B'' - A' = \lambda(B - A) \Rightarrow \|B'' - A'\|_2 = \lambda \|B - A\|_2.$$

But since B' is the projection of A' onto K , we obtain:

$$\|B' - A'\|_2 \leq \|B'' - A'\|_2 = \lambda \|B - A\|_2 \Rightarrow \|B' - A'\|_2 < \|B - A\|_2.$$

■

We split the proof of stability in two parts: first we show that Algorithm 1 brings the out-of-plane related entries D_y to an element of S_{D_y} ; then we prove that Algorithm 1 brings the in-plane related entries D_{xz} to an element of $S_{D_{xz}}$:

3.1.1 Convergence of the out-of-plane motion:

In the following proposition, the sequence $(\phi_k)_{k \in \mathbb{N}}$ represents the iterative application of the control Algorithm 1 on the state D_y related to the out-of-plane motion:

Proposition 3.5 (Convergence of the out-of-plane trajectory). *Let be $D_y \in \mathbb{R}^2$, $\nu, \tau_I, \tau_S \in \mathbb{R}_{>0}$ s.t. $\forall k \in \mathbb{Z}_{>0}$, $\tau_I \neq k\pi$, $N \geq 3$ and $S_{D_y} \neq \emptyset$. Then, the following sequence:*

$$(\phi_k)_{k \in \mathbb{N}} := \begin{cases} \phi_0 = D_y, \\ \phi_k = \phi_{k-1} + M_y(\nu_k^{(1)}, \dots, \nu_k^{(N)}) \Delta V_{y_k}, & \text{if } \|\Delta V_{y_k}\|_\infty \leq \overline{\Delta V} \\ \phi_k = \phi_{k-1} + M_y(\nu_k^{(1)}, \dots, \nu_k^{(N)}) \gamma_{\overline{\Delta V}}(\Delta V_{y_k}), & \text{if } \|\Delta V_{y_k}\|_\infty > \overline{\Delta V} \end{cases},$$

where $\nu_k^{(i)} = \nu + (i-1)\tau_I + (k-1)\tau_S$ and $\Delta V_{y_k} = \gamma_y(\phi_{k-1}, \nu_k^{(1)}, \dots, \nu_k^{(N)})$, converges to an element of S_{D_y} .

Proof. From Proposition 3.2, the function γ_y returns a sequence of impulses that generates an admissible trajectory, i.e. $\phi_k = \phi_{k-1} + M_y(\nu_k^{(1)}, \dots, \nu_k^{(N)}) \Delta V_{y_k} \in S_{D_y}$. Then, if for some k^* the impulse $\Delta V_{y_{k^*}}$ respects the saturation constraint, we have that $\forall k \geq k^*$, $\phi_k \in S_{D_y}$.

However, suppose that the saturation is always violated for any $k \in \mathbb{N}$ (worst case scenario). By writing the expressions of ϕ_k considering the non-scaled and the scaled sequence of impulses, we obtain:

$$\begin{aligned} \bar{\phi}_k &= \phi_{k-1} + M_y(\nu_k^{(1)}, \dots, \nu_k^{(N)}) \Delta V_{y_k} \\ \phi_k &= \phi_{k-1} + M_y(\nu_k^{(1)}, \dots, \nu_k^{(N)}) \Delta V_{y_k} \overline{\Delta V} / \|\Delta V_{y_k}\|_\infty \end{aligned}$$

By manipulating the previous equations, we obtain the following expression:

$$\bar{\phi}_k - \phi_k = (1 - \overline{\Delta V} / \|\Delta V_{y_k}\|_\infty) (\bar{\phi}_k - \phi_{k-1})$$

From the saturation hypothesis we have that $\overline{\Delta V} < \|\Delta V_{y_k}\|_\infty$ and consequently:

$$\|\bar{\phi}_k - \phi_k\|_2 = (1 - \overline{\Delta V} / \|\Delta V_{y_k}\|_\infty) \|\bar{\phi}_k - \phi_{k-1}\|_2 < \|\bar{\phi}_k - \phi_{k-1}\|_2$$

Since $\bar{\phi}_k$ belongs to S_{D_y} , which is a convex set, from Proposition 3.4 we conclude that:

$$\text{dist}_{S_{D_y}}(\phi_k) \leq (1 - \overline{\Delta V} / \|\Delta V_{y_k}\|_\infty) \text{dist}_{S_{D_y}}(\phi_{k-1}) < \text{dist}_{S_{D_y}}(\phi_{k-1})$$

We then define the following sets:

$$P_k := \left\{ D \in \mathbb{R}^2 \mid \text{dist}_{S_{D_y}}(D) \leq \text{dist}_{S_{D_y}}(\phi_{k-1}) \right\},$$

$$Q_k := \{ \Delta V_y \in \mathbb{R}^2 \mid \exists \nu \in \mathbb{R}, \exists D \in P_k \text{ s.t. } \Delta V_y = \gamma_y(D, \nu, \dots, \nu + (N-1)\tau_I) \},$$

and $\Delta V_{y_k}^* := \max_{\Delta V_y \in Q_k} \|\Delta V_y\|_\infty$. One can remark that since $\text{dist}_{S_{D_y}}(\phi_k) < \text{dist}_{S_{D_y}}(\phi_{k-1})$, the sets Q_k form a sequence of inclusions $Q_{k+1} \subseteq Q_k$ and, consequently, $\Delta V_{y_{k+1}}^* \leq \Delta V_{y_k}^*$. Now let us define the following two sequences:

$$(a_k)_{k \in \mathbb{N}} := \begin{cases} a_0 = \text{dist}_{S_{D_y}}(\phi_0), \\ a_k = \alpha a_{k-1} \end{cases} \quad \text{and} \quad (b_k)_{k \in \mathbb{N}} := \begin{cases} b_0 = \text{dist}_{S_{D_y}}(\phi_0) \\ b_k = \text{dist}_{S_{D_y}}(\phi_{k-1}) \end{cases}$$

where $\alpha = (1 - \overline{\Delta V} / \Delta V_{y_1}^*)$. The sequence $(a_k)_{k \in \mathbb{N}}$ has a general term of the form $a_k = \alpha^k a_0$ and converges to zero when k tends to infinite: $\alpha < 1 \Rightarrow a_k \xrightarrow{k \rightarrow \infty} 0$. The second sequence represents the distance of the terms of the sequence ϕ_k to the admissible set S_{D_y} . Since we suppose that the saturation is always violated, we have the following inequalities:

$$\overline{\Delta V} < \|\Delta V_{y_k}\|_\infty < \Delta V_{y_k}^* \leq \Delta V_{y_1}^*, \quad \forall k \in \mathbb{N}$$

Then, since $\text{dist}_{S_{D_y}}(\phi_k) \leq (1 - \overline{\Delta V} / \|\Delta V_{y_k}\|_\infty) \text{dist}_{S_{D_y}}(\phi_{k-1})$ and $\forall k \in \mathbb{N}$, $(1 - \overline{\Delta V} / \|\Delta V_{y_k}\|_\infty) < \alpha$, by comparing the sequences $(a_k)_{k \in \mathbb{N}}$ and $(b_k)_{k \in \mathbb{N}}$ we prove that $b_k \xrightarrow{k \rightarrow \infty} 0$, which is equivalent to $\text{dist}_{S_{D_y}}(\phi_k) \xrightarrow{k \rightarrow \infty} 0$. ■

By demonstrating that the sequence $(\phi_k)_{k \in \mathbb{N}}$ converges to a point in the admissible set we prove that the MPC strategy is convergent for the out-of-plane motion.

3.1.2 Convergence of the in-plane motion:

If the initial state D_{xz} is not periodic and Algorithm 1 does not produce a sequence of impulses that respects the saturation threshold, the while loop described in lines 10-23 is executed with the goal of generating a periodic trajectory. In the following proposition, the sequence $(\theta_k)_{k \in \mathbb{N}}$ represents the behavior of the first entry of the state vector D_{xz} during the execution of this while loop:

Proposition 3.6 (Convergence to a periodic trajectory). *Let be $d_{0_{xz}} \in \mathbb{R}$, $\nu \in \mathbb{R}$, $\tau_P \in \mathbb{R}_{>0}$. Then, the sequence $(\theta_k)_{k \in \mathbb{N}}$ defined by:*

$$(\theta_k)_{k \in \mathbb{N}} := \begin{cases} \theta_0 = d_{0_{xz}}, \\ \theta_k = \theta_{k-1} + M_0(\nu_k) \Delta V_{xz_k}, & \text{if } \|\Delta V_{xz_k}\|_\infty \leq \overline{\Delta V} \\ \theta_k = \theta_{k-1} + M_0(\nu_k) \gamma_{\overline{\Delta V}}(\Delta V_{xz_k}), & \text{if } \|\Delta V_{xz_k}\|_\infty > \overline{\Delta V} \end{cases},$$

where $\Delta V_{xz_k} = \gamma_P(\theta_{k-1}, \nu_k)$ and $\nu_k = \nu + (k-1)\tau_P$, converges to 0.

Proof. The proof is *mutatis mutandis* similar to that presented in Proposition 3.5. ■

By demonstrating that the sequence $(\theta_k)_{k \in \mathbb{N}}$ converges to zero, we prove that iterative calls of the MPC strategy produces a periodic trajectory. Once the trajectory becomes periodic, the behavior of the state D_{xz} under iterative calls of Algorithm 1 can be represented by the sequence $(\varphi_k)_{k \in \mathbb{N}}$ introduced in the following proposition:

Proposition 3.7 (Convergence of the in-plane trajectory). *Let be $D_{xz} \in \mathbb{R}^4$ s.t. $d_{0_{xz}} = 0$, $\nu, \tau_I, \tau_S \in \mathbb{R}_{>0}$ s.t. $\forall k \in \mathbb{Z}_{>0}$, $\tau_I \neq k\pi$, $N \geq 3$ and $S_{D_{xz}} \neq \emptyset$. Then, the following sequence:*

$$(\varphi_k)_{k \in \mathbb{N}} := \begin{cases} \varphi_0 = D_{xz}, \\ \varphi_k = \varphi_{k-1} + M_{xz}(\nu_k^{(1)}, \dots, \nu_k^{(N)}) \Delta V_{xz_k}, & \text{if } \|\Delta V_{y_k}\|_\infty \leq \overline{\Delta V} \\ \varphi_k = \varphi_{k-1} + M_{xz}(\nu_k^{(1)}, \dots, \nu_k^{(N)}) \gamma_{\overline{\Delta V}}(\Delta V_{xz_k}), & \text{if } \|\Delta V_{xz_k}\|_\infty > \overline{\Delta V} \end{cases},$$

where $\nu_k^{(i)} = \nu + (i-1)\tau_I + (k-1)\tau_S$ and $\Delta V_{xz_k} = \gamma_{xz}(\varphi_{k-1}, \nu_k^{(1)}, \dots, \nu_k^{(N)})$, converges to an element of $S_{D_{xz}}$.

Proof. The proof is *mutatis mutandis* similar to that presented in Proposition 3.5. ■

By demonstrating that the sequence $(\varphi_k)_{k \in \mathbb{N}}$ converges to a point in the admissible set, we prove that the MPC strategy is convergent for the in-plane motion.

3.1.3 Invariance

So far we established the convergence of the vector of parameters to an element of the admissible set. Now let us prove that once an admissible trajectory is obtained, it is preserved by the proposed model predictive control algorithm. But first, let notice that the S_D is naturally invariant as a subset of the invariant set of periodic orbits.

Proposition 3.8 (Invariance). *The set S_D is invariant under the action of the instructions defined in Algorithm 1.*

Proof. This is evident: since $D \in S_D \Rightarrow d_0 = 0$ (periodicity), the function γ_p is never called; the functions γ_y and γ_{xz} compute the fuel-optimal sequence of impulses that generate a trajectory respecting the out-of-plane and the in-plane space constraints respectively. But since

$$D \in S_D \Rightarrow \underline{x} \leq x(\nu) \leq \bar{x}, \underline{y} \leq y(\nu) \leq \bar{y}, \underline{z} \leq z(\nu) \leq \bar{z}, \forall \nu,$$

the functions will return a null sequence of impulses. ■

4 Finite descriptions of the space constraints

As previously discussed in Section 2.2, the infinitely many affine inequalities in the description of the admissible set (see Eq. 2.11) are hard to be accounted in practice. Moreover, although the functions γ_y and γ_{xz} in (3.4) and (3.5) were defined as the solutions of optimization problems whose the feasible sets are the projections of the admissible set in the out-of-plane and in-plane directions, practical ways to compute these solutions were not discussed. Hereafter, we present two different finite descriptions for the admissible set and the respective methods employed on the resolution of the their associated fuel-optimal impulsive optimization problems.

4.1 SDP description of periodic space constrained relative trajectories

Deaconu presents in [8, 9, 10] a finite mathematical description of the periodic relative trajectories respecting polytopic space constraint. This description is obtained by performing a variable change that converts each one of the "belonging to one side of the plane" constraints into one polynomial non-negative constraint; after that, we apply the result demonstrated by Nesterov in [26], that links the univariate polynomial non-negativity to the existence of a semi-definite positive matrix whose entries are related to the coefficients of the polynomial. By performing variable changes, the space-constraints inequalities in (2.3) can then be reformulated as:

$$\Gamma_{\underline{x}}(s) \geq 0, \quad \Gamma_{\bar{x}}(s) \geq 0, \quad \Gamma_{\underline{y}}(s) \geq 0, \quad \Gamma_{\bar{y}}(s) \geq 0, \quad \Gamma_{\underline{z}}(s) \geq 0, \quad \Gamma_{\bar{z}}(s) \geq 0, \quad \forall s \in \mathbb{R}. \quad (4.1)$$

Let be γ_w the vector of coefficients of the polynomial Γ_w in (4.1). Applying Nesterov results [26, Theorem 17.10], we finally obtain the following novel description for the admissible set:

$$S_D = \{D \in \mathbb{R}^6 \mid d_0 = 0, \exists Y_w \succeq 0 \text{ s.t. } \gamma_w = \Lambda^*(Y_w), w \in \{\underline{x}, \bar{x}, \underline{y}, \bar{y}, \underline{z}, \bar{z}\}\} \quad (4.2)$$

where the operator Λ^* is defined by:

$$\Lambda^*(Y)(j) = \text{tr}(Y H_{m,j}), \quad j = 1, \dots, 2m + 1 \quad (4.3)$$

and $H_{m,j} \in \mathbb{R}^{(m+1) \times (m+1)}$ are the Hankel matrices that contain ones on the j -th anti-diagonal and zeros elsewhere. The associated fuel-optimal impulsive optimization problem is formulated as follows:

Problem 2. Given $N \geq 3$, $\nu_1 < \dots < \nu_N \in \mathbb{R}_{>0}$, $D(\nu_1) \in \mathbb{R}^6$, $e, a, \mu \in \mathbb{R}$, find $\Delta V^* \in \mathbb{R}^{3N}$ such that:

$$\begin{aligned} \Delta V^* = & \underset{\Delta V}{\text{argmin}} \quad J(\Delta V) \\ \text{s.t.} \quad & \begin{cases} D(\nu_1) = D_1 \\ D^+(\nu_N) = \Phi_D(\nu_N, \nu_1)D(\nu_1) + M(\nu_1, \dots, \nu_N) \Delta V \\ d_0^+(\nu_N) = 0 \\ \exists Y_w \succeq 0 \text{ s.t. } \gamma_w(D^+(\nu_N)) = \Lambda^*(Y_w), \quad w \in \{\underline{x}, \bar{x}, \underline{y}, \bar{y}, \underline{z}, \bar{z}\} \end{cases} \quad (\mathcal{P}.\text{SDP}) \end{aligned}$$

This problem can be solved by dedicated semi-definite program (SDP) solvers (SDPA, SeDuMi, SDPT3, CSDP, etc).

4.2 Envelope description of periodic space constrained relative trajectories

In [3] a redefinition of the set of periodic space-constrained trajectories based on the evaluation of convex semi-algebraic functions is provided by finding the envelope of the curves defining the boundary of the

so-called admissible set. Therein, the periodic vectors of parameters $D \in \mathbb{R}^6$, *s.t.* $d_0 = 0$ respecting the space-constraints inequalities (2.3) are such that:

$$g_{\underline{x}}(D) \leq 0, \quad g_{\bar{x}}(D) \leq 0, \quad g_{\underline{y}}(D) \leq 0, \quad g_{\bar{y}}(D) \leq 0, \quad g_{\underline{z}}(D) \leq 0, \quad g_{\bar{z}}(D) \leq 0, \quad (4.4)$$

where the functions $g_w(D)$ are convex but non-differentiable functions. Hence the admissible set can be redefined as:

$$S_D = \{ D \in \mathbb{R}^6 \mid d_0 = 0, \quad g_w(D) \leq 0, \quad w \in \{\underline{x}, \bar{x}, \underline{y}, \bar{y}, \underline{z}, \bar{z}\} \} \quad (4.5)$$

and the associated fuel-optimal impulsive optimization problem:

Problem 3. *Given $N \geq 3$, $\nu_1 < \dots < \nu_N \in \mathbb{R}_{>0}$, $D(\nu_1) \in \mathbb{R}^6$, $e, a, \mu \in \mathbb{R}$, find $\Delta V^* \in \mathbb{R}^{3N}$ such that:*

$$\begin{aligned} \Delta V^* = \underset{\Delta V}{\operatorname{argmin}} \quad & J(\Delta V) \\ \text{s.t.} \quad & \begin{cases} D(\nu_1) = D_1 \\ D^+(\nu_N) = \Phi_D(\nu_N, \nu_1)D(\nu_1) + M(\nu_1, \dots, \nu_N) \Delta V \\ d_0^+(\nu_N) = 0 \\ g_w(D^+(\nu_N)) \leq 0, \quad w \in \{\underline{x}, \bar{x}, \underline{y}, \bar{y}, \underline{z}, \bar{z}\} \end{cases} \quad (\mathcal{P}.ENV) \end{aligned}$$

This problem is characterized by convex but non-differentiable functions in its criterion and in the description of its feasible set. It can be converted into an unconstrained optimization problem via penalty methods and the resulting problem can be solved by sub-gradient methods (see [3] for details).

5 Simulations and Results

Hereafter we present the results obtained by employing the proposed MPC algorithm to control the relative motion between spacecraft during the rendezvous hovering phases.

5.1 Hardware-in-the-loop simulations

The tests are performed in a hardware-in-the-loop environment: each call of the MPC algorithm is executed on a board dedicated to space application; the computed control actions are sent via network connection to a computer running a Matlab/Simulink model that simulates the relative dynamics between spacecraft (see Fig. 6).

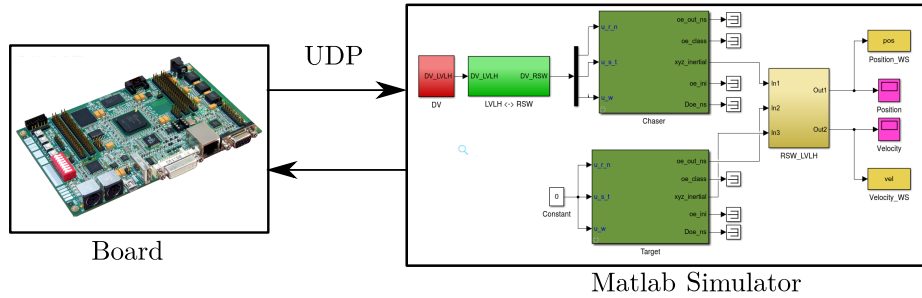


Figure 6: Hardware-in-the-loop environment: network connection between board and simulator via user datagram protocol.

5.1.1 Software

Both the SDP and the envelope (hereafter we use the abbreviation ENV) approaches are adopted to model the fuel-optimal control problem. The SDP problems are solved via the CSDP solver [5], using the standard options and parameters. The envelope problems are solved by a combination of penalty method with iterative optimization algorithms based on sub-gradients: the constraints are weighted by a coefficient equivalent to 10^8 and added to the objective function and the resulting unconstrained problem is solved by performing (at most) 50 iterations of the BFGS method¹ presented by Lewis and Overton [19, Algorithm 2.1], followed by 500 iterations of the sub-gradient method presented by Shor [31, Theorem 2.2] (see [3] for details). All embedded programs are coded in C.

¹A version of the algorithm HANSO v2.2 translated to C is used (<http://www.cs.nyu.edu/overton/software/hanso/>).

5.1.2 Hardware

The board is an AEROFLEX GAISLER GR-XC6S that contains a synthesized LEON3 microprocessor [27] and supports a IEEE-754 compliant floating-point unit with single and double precision (32 and 64-bit floats). It has a 128 Mbyte DDR2 RAM, a 8 Mbyte PROM and a 8 Mbyte SPI PROM memories and runs a Linux 2.6 environment that simulates the performance of devices usually employed in space applications [12]. The embedded libraries occupy 12 Mbyte and the C binary executables have 44 Kbyte (ENV) and 148 Kbyte (SDP).

5.1.3 Simulating the relative dynamics

Two types of simulator are used: a linear simulator computing the evolution of the relative motion via the propagation of the vector of parameters presented in equations 2.26; and a nonlinear simulator [1] based on the Gauss planetary equations for the relative motion [33, 34] that takes into account the effects of disturbances, such as the atmospheric drag, Earth's oblateness, uncertainties on the measurement of the relative state (we consider a white noise on position and velocity characterized by the following standard deviation: $d_p = 10^{-2}$ m, $d_v = 10^{-5}$ m/s), execution errors on the orientation and magnitude of applied impulsive velocity corrections (we consider a mismatch of $\pm 1^\circ$ in orientation and $\pm 1\%$ in magnitude). The linear simulations are performed in order to verify the theoretical results about the stability of the proposed algorithm. The nonlinear simulations assess the robustness of the proposed algorithm under disturbances and nonlinearities that are not taken into account by the linear model.

5.1.4 Scenarios

In order to compare the obtained results to those presented in [7], the same scenarios (based on the PRISMA mission [4]) are studied: Earth's gravitational constant: $\mu = 3.986004418 \cdot 10^{14}$; leader's orbital parameters: $e = 0.004$, $a = 7011$ km, $i = 98^\circ$, $\Omega = 0^\circ$, $\omega = 0^\circ$; leader's initial true anomaly $\nu_0 = 0^\circ$; number of impulses adopted is $N = 3$; true anomaly interval between impulses $\tau_I = 120^\circ$; true anomaly interval between sequence of impulses $\tau_S = 120^\circ$; true anomaly interval to achieve periodicity $\tau_P = 3, 6^\circ$; space constraints: $\underline{x} = 50$, $\bar{x} = 150$, $\underline{y} = -25$, $\bar{y} = 25$, $\underline{z} = -25$, $\bar{z} = 25$; propellers saturation threshold: 0.5 m/s; duration of simulation: 10 orbital periods; initial relative state:

$$\begin{aligned} X_{01} &= [400, 300, -40, 0, 0, 0]^T \\ X_{02} &= [-800, 600, 200, 0, 0, 0]^T \\ X_{03} &= [-1500, 1300, 150, 0, 0, 0]^T \\ X_{04} &= [5000, 1300, 500, 0, 0, 0]^T \end{aligned},$$

where the first three components of each vector represent the relative LVLH positions (in meters) and the last three, the relative LVLH velocities (in meters per second);

5.2 Results analysis

5.2.1 Convergence definition

To evaluate the convergence, we extend the use the mismatch ratio η presented in [7]. The mismatch ratio is given by:

$$\eta(\nu) = \frac{\text{dist}_{S_D} D(\nu)}{\text{dist}_{S_D} D(\nu_0)} = \frac{\text{dist}_{S_D} C(\nu)T(\nu)D(\nu)}{\text{dist}_{S_D} C(\nu_0)T(\nu_0)D(\nu_0)}, \quad (5.1)$$

which is the ratio between the distance to the admissible set of the current and initial vector of parameters. For a given $\delta \in [0, 1]$ the convergence time T_c is defined as:

$$T_c(\delta) \in \mathbb{R}_{>0} \text{ s.t. } \forall \nu \geq T_c, \eta(\nu) \leq \delta, \quad (5.2)$$

and we set δ to 5%.

5.2.2 Consumption, convergence time and running time

Convergence ($\delta < 5\%$) and hovering are obtained for all performed simulations. Table 1, present the obtained fuel-consumption J . From this point of view, the SDP-based controller is the most performing with respect to the ENV-based controller. This is due to the fact that the limited number of iterations of the BFGS and sub-gradient algorithms generate suboptimal solutions of ($\mathcal{P}.ENV$), while the SDP approach always returns the optimal solution of ($\mathcal{P}.SDP$). Nevertheless, both approaches engender fuel-consumptions that are approximatively half of the lower values produced by any of the three control laws proposed in [7].

Convergence times T_c for each simulations are reported in Table 2. The non linear simulation environment has little impact on convergence performances except for the initial condition X_{04} . Comparing with the hybrid controller developed in [7], the proposed approaches are not generally the best. For instance, for X_{01} the control law B in [7] generates a convergence time equal to 0.34 orbits, while the proposed SDP and ENV approaches take twice as much time to converge. This indicates that the strategy that we propose gives more emphasis to reducing the consumption than producing short convergence times. Besides, when the initial condition recede from the hovering zone, the MPC controller abilities to account for input constraints permit to ensure the convergence and limit the convergence time. On the other hand, the behavior of hybrid controllers is degraded in terms of convergence and consumption due to the presence of the saturation (one of the examples of application of the hybrid controller even diverges).

Table 1: Consumption J (m/s)

Initial condition	SDP		ENV	
	LIN	NLIN	LIN	NLIN
X_{01}	0.45	0.47	0.53	0.58
X_{02}	1.20	1.25	1.31	1.32
X_{03}	2.21	2.26	2.31	2.38
X_{04}	4.75	4.71	5.41	6.69

Table 2: Convergence time T_c (number of orbits)

Initial condition	SDP		ENV	
	LIN	NLIN	LIN	NLIN
X_{01}	0.66	0.66	0.64	0.69
X_{02}	0.66	0.66	0.64	0.69
X_{03}	1.65	1.65	1.65	1.65
X_{04}	2.69	1.70	1.67	2.66

Table 3 and 4 permit to compare the numerical performance both SDP and ENV based controllers. For both approaches, the average time to compute a sequence of $N = 3$ impulses is lower than 3.0 seconds and the maximal running time is never longer than 4.0 seconds (this time is negligible when compared to the orbital period $T = 2\pi\sqrt{a^3/\mu} \approx 5842$ seconds). Moreover, the amount of memory allocated by the execution of the binaries are 5056 Kbyte for the SDP approach and 5584 Kbyte for the ENV approach - these are reasonable values compared to the available memory of approximatively 90 Mbyte.

Table 3: Average running time (s)

Initial condition	SDP		ENV	
	LIN	NLIN	LIN	NLIN
X_{01}	2.82	2.94	0.30	2.71
X_{02}	2.82	2.86	0.31	2.68
X_{03}	2.83	2.87	0.41	2.52
X_{04}	2.70	2.89	1.54	2.81

Table 4: Maximal running time (s)

Initial condition	SDP		ENV	
	LIN	NLIN	LIN	NLIN
X_{01}	2.93	3.31	3.05	2.91
X_{02}	2.96	3.23	3.07	3.09
X_{03}	2.93	3.05	3.23	3.12
X_{04}	2.79	3.54	3.29	3.37

5.2.3 Relative trajectories, impulses and distance to the admissible set

In Figures 7 - 10, we show the resulting 3D relative trajectories (we zoom into the hovering region), the computed and applied impulses for the nonlinear simulations and the evolution of the mismatching ratio $\eta(\nu)$ for the initial conditions X_{03} and X_{04} . By observing the relative trajectories obtained for the linear simulations, we notice that the relative movement converges to a periodic trajectory included in the hovering zone and, once this trajectory is reached, it remains unchanged - this fact illustrates the convergence and invariance results demonstrated in Prop. 3.5 - 3.8. The same behavior, however, is not observed for nonlinear simulations: due to the presence of disturbances and uncertainties, the control actions are not able to produce perfect periodic orbits. This is also observed in Fig. 11a where for the nonlinear simulation, the mismatch ratio oscillates close to zero, but never reaches it. Moreover,

although some impulses are saturated (Fig. 7b, 8b, 9b and 10b), the convergence is achieved for both linear and nonlinear simulations.

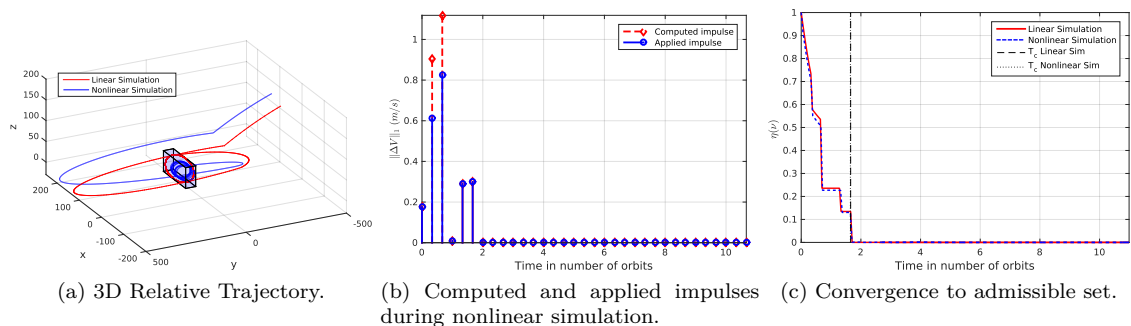


Figure 7: Results for trajectory X_{03} (SDP approach).

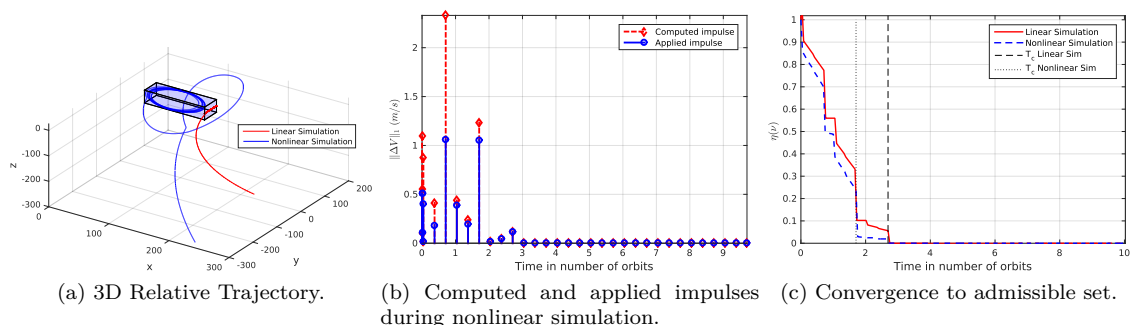


Figure 8: Results for trajectory X_{04} (SDP approach).

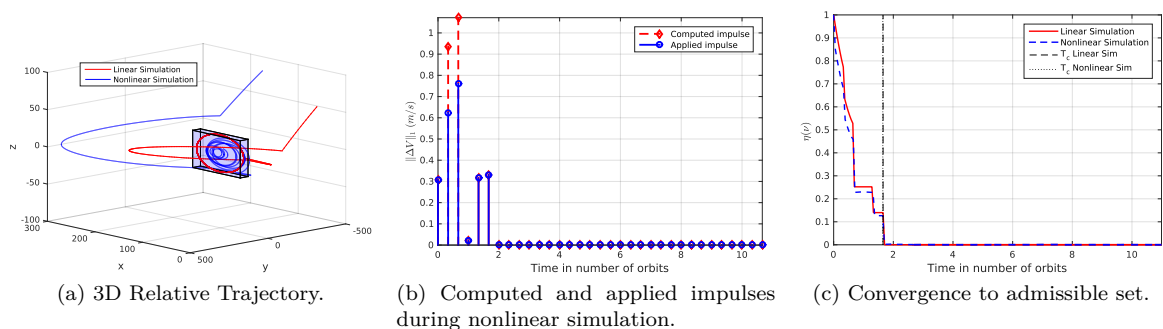


Figure 9: Results for trajectory X_{03} (ENV approach).

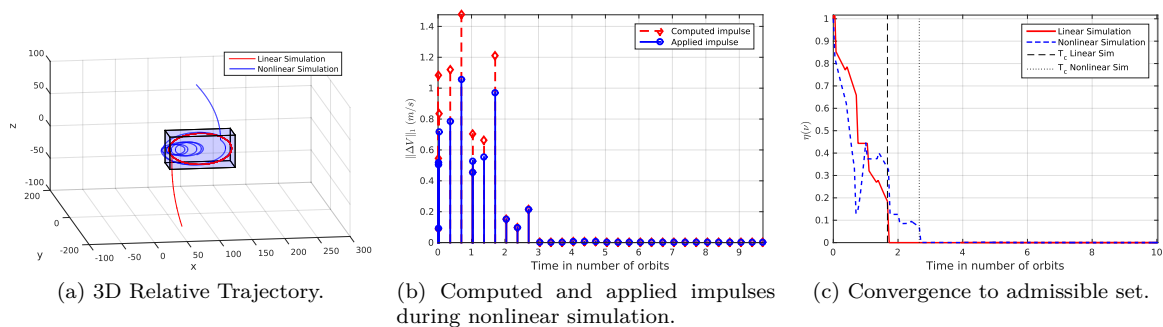


Figure 10: Results for trajectory X_{04} (ENV approach).

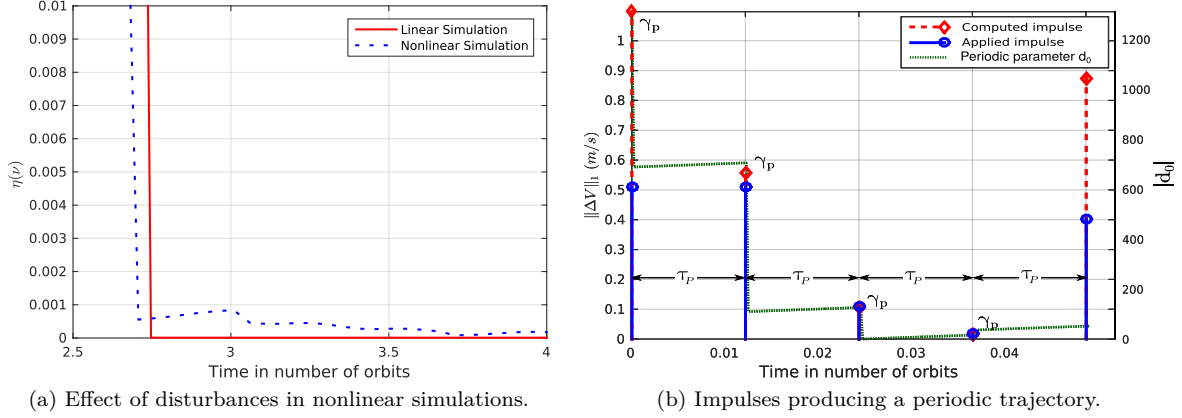


Figure 11: Details of results obtained for trajectory X_{04} (SDP approach).

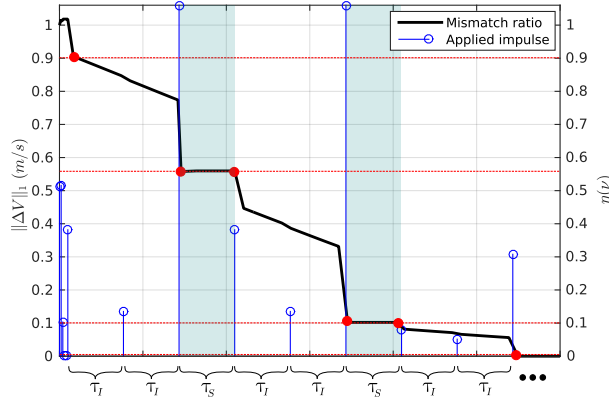


Figure 12: Trajectory X_{04} , linear simulation. Decrease of the mismatch ratio after each sequence of 3 impulses (SDP approach).

In Fig. 11b we show in details the four initial impulses applied in order to reduce the absolute value of d_0 (these impulses are computed via γ_p and are separated by true anomaly intervals of τ_P , indicated in the figure; for nonlinear simulations, due to the disturbances, the condition $d_0 = 0$ is never reached, being therefore replaced by another condition $|d_0| < \text{threshold}$). In Fig. 12 we show that after each sequence of $N = 3$ impulses, the distance to the admissible set decreases (indicated by the dotted lines). Furthermore, during the interval between sequences of impulses (indicated by τ_S and the shaded zones), the mismatch ratio remains constant.

5.2.4 Impact of parameters on fuel-consumption

Hereafter we study the effect of some parameters (eccentricity, number of impulses, initial true anomaly and the three true anomaly intervals τ_P , τ_I , τ_S) on the total fuel-consumption. We perform linear simulations using the SDP approach for the four initial states $X_{01} - X_{04}$; one single parameter varies at time and the others are kept at the same values employed in the previous simulations. The obtained results are presented in Fig. 14 - 18.

Fig. 13 indicates that a small number of impulses should be chosen, since the fuel-consumption increases with the growth of this parameter. The augmentation of the fuel-consumption with the increase of the eccentricity (Fig. 14) or with the reduction of the interval between impulses (Fig. 15) are consistent with results previously presented in the literature [8, Section 6.4]. Different choices of initial true anomaly produce a sinusoidal profile for the fuel-consumption, which implies the existence of a fuel-optimal choice for the initial firing instant ν_0 (Fig. 16). In Fig. 17, the consumption increases until it reaches its maximum around $\tau_p = 2.4^\circ$ or 0.042 rad, then starts to decrease; in order to minimize consumption and convergence time, this parameter should be set to the smallest value possible, which is defined by the physical limitations of the spacecraft propellers. The profile of consumption obtained by varying the

interval between sequences of impulses does not present a particular shape or behavior and therefore no general conclusion can be obtained from it (Fig. 18). **Remark:** in Fig. 16 - 18, for each initial state, the fuel-consumptions are normalized between 0 and 1.

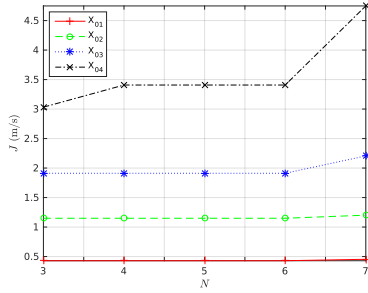


Figure 13: Impact of number of impulses on fuel-consumption.

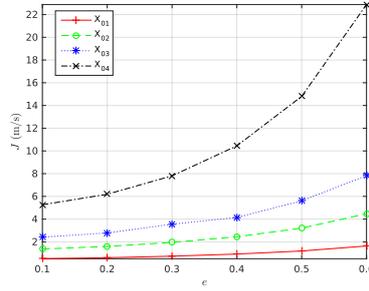


Figure 14: Impact of eccentricity on fuel-consumption.

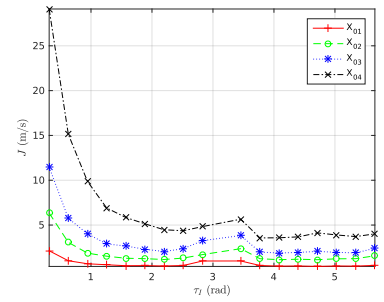


Figure 15: Impact of true anomaly interval between impulses on fuel-consumption.

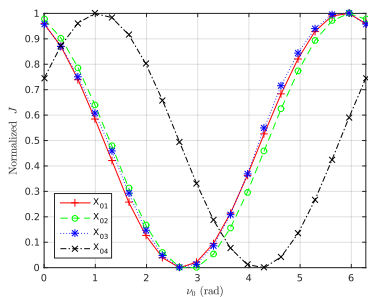


Figure 16: Impact of initial true anomaly on fuel-consumption.

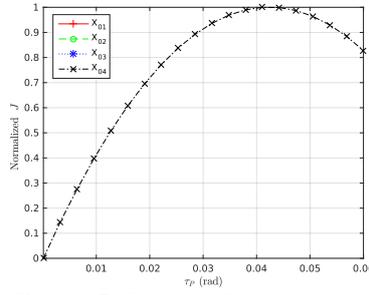


Figure 17: Impact of true anomaly interval between impulses to generate periodic trajectories on fuel-consumption

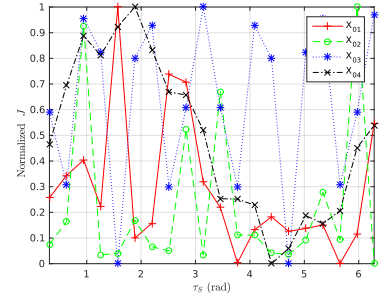


Figure 18: Impact of true anomaly interval between sequences of impulses on fuel-consumption

6 Conclusions

In this article, a new model predictive control strategy is proposed for the impulsive spacecraft rendezvous hovering phases. A theoretical stability proof is provided, demonstrating that, even when the saturation of the propellers is taken into account, the proposed strategy produces a sequence of control actions generating a periodic relative trajectory included in the hovering region.

Hardware-in-the-loop simulations using a LEON3 synthesized microprocessor reveal that although the proposed approach may produce greater convergence times, it is more efficient with respect to fuel-consumption than other methods proposed in the literature. Moreover, the timings obtained during these tests bring out the fact that this approach can be efficiently embedded in space dedicated devices. Finally, an analysis of the impact of the parameters rendezvous scenarios on the fuel-consumption is also presented.

Future works should focus in investigating the robustness of the proposed controller from a theoretical point of view, providing, for example, an idea of the influence of the nonlinearities, disturbances and scenario parameters on the stability of the method.

Acknowledgments

This work was supported by the FastRelax (ANR-14-CE25-0018-01) project of the French National Agency for Research (ANR).

References

- [1] P. R. Arantes Gilz. A Matlab®/Simulink® non-linear simulator for orbital spacecraft rendezvous applications., December 2016. URL <https://hal.archives-ouvertes.fr/hal-01413328>. A Matlab®/Simulink® non-linear simulator for orbital spacecraft rendezvous applications.
- [2] P. R. Arantes Gilz and C. Louembet. Predictive control algorithm for spacecraft rendezvous hovering phases. In *Control Conference (ECC), 2015 European*, pages 2085–2090. IEEE, 2015.
- [3] P. R. Arantes Gilz, M. Joldes, C. Louembet, and F. Camps. Model predictive control for rendezvous hovering phases based on a novel description of constrained trajectories. In *IFAC World Congress*, pages pp. 7490–7495, Toulouse, France, July 2017. URL <https://hal.laas.fr/hal-01484764>.
- [4] P. Bodin, R. Larsson, F. Nilsson, C. Chasset, R. Noteborn, and M. Nylund. Prisma: an in-orbit test bed for guidance, navigation, and control experiments. *Journal of Spacecraft and Rockets*, 46(3):615, 2009.
- [5] B. Borchers. CSDP, A C library for semidefinite programming. *Optimization Methods and Software*, 11(1-4):613–623, 1999.
- [6] L. S. Breger, G. Inalhan, M. Tillerson, and J. P. How. *Cooperative Spacecraft Formation Flying: Model Predictive Control with Open- and Closed-Loop Robustness*, volume 1 of *Elsevier Astrodynamics Series*, pages 237 – 277. Butterworth-Heinemann, 2006.
- [7] M. Brentari, D. Arzelier, C. Louembet, S. Urbina, and L. Zaccarian. A hybrid control framework for impulsive control of satellite rendezvous. In *2016 American Control Conference (ACC)*, pages 7414–7419, July 2016. doi: 10.1109/ACC.2016.7526843.
- [8] G. Deaconu. *On the trajectory design, guidance and control for spacecraft rendezvous and proximity operations*. PhD thesis, Univ. Toulouse 3 - Paul Sabatier, Toulouse, France, October 2013.
- [9] G. Deaconu, C. Louembet, and A. Théron. Minimizing the effects of navigation uncertainties on the spacecraft rendezvous precision. *Journal of Guidance, Control, and Dynamics*, 37(2):695–700, February 2014. ISSN 0731-5090. doi: 10.2514/1.62219. URL <https://doi.org/10.2514/1.62219>.
- [10] G. Deaconu, C. Louembet, and A. Théron. Designing continuously constrained spacecraft relative trajectories for proximity operations. *Journal of Guidance, Control, and Dynamics*, 38(7):1208–1217, 2015.
- [11] S. Di Cairano, H. Park, and I. Kolmanovsky. Model predictive control approach for guidance of spacecraft rendezvous and proximity maneuvering. *International Journal of Robust and Nonlinear Control*, 22(12):1398–1427, 2012. ISSN 1099-1239. doi: 10.1002/rnc.2827. URL <http://dx.doi.org/10.1002/rnc.2827>.
- [12] ESA. Onboard computer and data handling, May 2014. URL <https://goo.gl/1PZNkC>. Accessed Nov. 17, 2017.
- [13] F. Gavilan, R. Vazquez, and E. F. Camacho. Chance-constrained model predictive control for spacecraft rendezvous with disturbance estimation. *Control Engineering Practice*, 20(2):111 – 122, 2012. ISSN 0967-0661. doi: <https://doi.org/10.1016/j.conengprac.2011.09.006>. URL <http://www.sciencedirect.com/science/article/pii/S0967066111001985>.
- [14] E. N. Hartley and J. M. Maciejowski. Predictive control for spacecraft rendezvous in an elliptical orbit using an FPGA. In *Control Conference (ECC), 2013 European*, pages 1359–1364. IEEE, 2013.
- [15] E. N. Hartley and J. M. Maciejowski. Field programmable gate array based predictive control system for spacecraft rendezvous in elliptical orbits. *Optimal Control Applications and Methods*, 36(5):585–607, 2015. ISSN 1099-1514. doi: 10.1002/oca.2117. URL <http://dx.doi.org/10.1002/oca.2117>.
- [16] D. J. Irvin, R. G Cobb, and T. A. Lovell. Fuel-optimal maneuvers for constrained relative satellite orbits. *Journal of guidance, control, and dynamics*, 32(3):960–973, 2009.
- [17] Y. Kuwata, A. Richards, and J. How. Robust receding horizon control using generalized constraint tightening. In *2007 American Control Conference*, pages 4482–4487, July 2007. doi: 10.1109/ACC.2007.4283000.
- [18] W. Langson, I. Chrysochoos, S.V. Raković, and D.Q. Mayne. Robust model predictive control using tubes. *Automatica*, 40(1):125 – 133, 2004. ISSN 0005-1098. doi: <https://doi.org/10.1016/j.automatica.2003.08.009>. URL <http://www.sciencedirect.com/science/article/pii/S0005109803002838>.
- [19] A. S. Lewis and M. L. Overton. Nonsmooth optimization via quasi-Newton methods. *Mathematical Programming*, 141(1-2):135–163, 2013.
- [20] D. Limon, I. Alvarado, T. Alamo, and E. F. Camacho. Robust tube-based mpc for tracking of constrained linear systems with additive disturbances. *Journal of Process Control*, 20(3):248 – 260, 2010. ISSN 0959-1524. doi: <https://doi.org/10.1016/j.jprocont.2009.11.007>. URL <http://www.sciencedirect.com/science/article/pii/S0959152409002169>.
- [21] F. Lobo Pereira, F. A. C. C. Fontes, A. Pedro Aguiar, and J. Borges de Sousa. *An Optimization-Based Framework for Impulsive Control Systems*, pages 277–300. Springer International Publishing, Cham, 2015. ISBN 978-3-319-26687-9. doi: 10.1007/978-3-319-26687-9_13. URL https://doi.org/10.1007/978-3-319-26687-9_13.

- [22] C. Louembet, D. Arzelier, and G. Deaconu. Robust rendezvous planning under maneuver execution errors. *Journal of Guidance, Control, and Dynamics*, 38(1):76–93, October 2015. ISSN 0731-5090. doi: 10.2514/1.G000391. URL <https://doi.org/10.2514/1.G000391>.
- [23] D. Q. Mayne, J. B. Rawlings, C. V. Rao, and P. O. M. Scokaert. Constrained model predictive control: Stability and optimality. *Automatica*, 36(6):789–814, 2000.
- [24] D. Q. Mayne, E. C. Kerrigan, and P. Falugi. Robust model predictive control: advantages and disadvantages of tube-based methods. In *18th IFAC World Congress*, volume 44, pages 191 – 196, 2011. doi: <https://doi.org/10.3182/20110828-6-IT-1002.01893>. URL <http://www.sciencedirect.com/science/article/pii/S1474667016436098>.
- [25] J. B. Mueller and R. Larsson. Collision avoidance maneuver planning with robust optimization. In *International ESA Conference on Guidance, Navigation and Control Systems, Tralee, County Kerry, Ireland, 2008*.
- [26] Y. Nesterov. Squared functional systems and optimization problems. In J.B.G. Frenk et al., editor, *High performance optimization*. Kluwer Academic Publishers, 2000.
- [27] PENDER. GR-XC6S Development Board - User Manual, July 2011. URL <https://goo.gl/SNt6vj>. Accessed Nov. 17, 2017.
- [28] A. Richards and J. P. How. Robust variable horizon model predictive control for vehicle maneuvering. *International Journal of Robust and Nonlinear Control*, 16(7):333–351, 2006. ISSN 1099-1239. doi: 10.1002/rnc.1059. URL <http://dx.doi.org/10.1002/rnc.1059>.
- [29] Pablo S. Rivadeneira, Antonio Ferramosca, and Alejandro H. González. Mpc with state window target control in linear impulsive systems. *IFAC-PapersOnLine*, 48(23):507 – 512, 2015. ISSN 2405-8963. doi: <https://doi.org/10.1016/j.ifacol.2015.11.329>. URL <http://www.sciencedirect.com/science/article/pii/S2405896315026130>. 5th IFAC Conference on Nonlinear Model Predictive Control NMPC 2015.
- [30] R. C. Shekhar and J. M. Maciejowski. Optimal constraint tightening policies for robust variable horizon model predictive control. In *2012 IEEE 51st IEEE Conference on Decision and Control (CDC)*, pages 5170–5175, Dec 2012. doi: 10.1109/CDC.2012.6426710.
- [31] N. Z. Shor. *Minimization methods for non-differentiable functions*, volume 3. Springer-Verlag, 1985.
- [32] J. Tschauner. Elliptic orbit rendezvous. *AIAA Journal*, 5(6):1110–1113, 1967.
- [33] D. A. Vallado. *Fundamentals of astrodynamics and applications*, volume 12. Springer, 2001.
- [34] M. J. H. Walker. A set of modified equinoctial orbit elements. *Celestial mechanics*, 38(4):391–392, 1986. ISSN 1572-9478.
- [35] K. Yamanaka and F. Ankersen. New state transition matrix for relative motion on an arbitrary elliptical orbit. *Journal of guidance, control, and dynamics*, 25(1):60–66, 2002.